Anisotropic optical spectra of doped manganites with pseudocubic perovskite structure

K. Tobe
Department of Applied Physics, University of Tokyo, Tokyo 113-8656, Japan
and Spin Superstructure Project, ERATO, JST, AIST Central 4, Tsukuba 305-8562, Japan

T. Kimura*
Department of Applied Physics, University of Tokyo, Tokyo 113-8656, Japan

Y. Tokura
Department of Applied Physics, University of Tokyo, Tokyo 113-8656, Japan
and Spin Superstructure Project, ERATO, JST, AIST Central 4, Tsukuba 305-8562, Japan
(Received 12 August 2003; revised manuscript received 4 November 2003; published 13 January 2004)

To investigate the effect of charge-spin-orbital correlations on electronic structures, anisotropic optical conductivity spectra have been investigated for twin-free crystals of various doped manganites $R_{1-x}A_x\mathrm{MnO_3}$ (R=Pr and Nd, A=Ca and Sr; $0.4 \leqslant x \leqslant 0.7$) with pseudo-cubic perovskite structure. In doped manganites having an antiferromagnetic ground state, a remarkable anisotropy has been observed in their optical spectra, reflecting the respective ferroic/antiferroic orders of e_g-orbital on Mn sites. Such orbital-order patterns give rise to characteristic optical spectra that show a strong spectral weight below ~ 2 eV with light polarization parallel to the direction of orbital lobes. Moreover, even in the ferromagnetic-metallic phases of $\mathrm{Pr_{1/2}Sr_{1/2}MnO_3}$ and $\mathrm{Nd_{1/2}Sr_{1/2}MnO_3}$, we observed substantial anisotropy in optical spectra. The results indicate the existence of orbital-polarized ferromagnetic-metallic phase in doped manganites although the ferromagnetic-metallic state attributed to the double-exchange interaction has been normally believed to accompany the orbital disordering.

DOI: 10.1103/PhysRevB.69.014407 PACS number(s): 75.47.Gk, 75.30.Et, 78.40.Ha

I. INTRODUCTION

Doped manganites with a perovskite structure, $R_{1-x}A_x\mathrm{MnO_3}$ (R and A being rare-earth and alkaline-earth ions, respectively), show a wide variety of magnetoelectronic phenomena such as colossal magnetoresistance (CMR) and a metal-insulator transition because of the mutual strong coupling among spin, charge, and orbital degrees of freedom of Mn d electrons.[1,2] The electronic configurations of the mixed-valent manganese ions ($\mathrm{Mn^{4+}}$ and $\mathrm{Mn^{3+}}$) are t_{2g}^3 and $t_{2g}^3 e_g^1$, respectively. In doped manganites, such configurations give rise to the coexistence and competition between the antiferromagnetic superexchange interaction produced by the half-filled t_{2g} orbitals and the ferromagnetic double-exchange interaction arising from the strong Hund's rule coupling between an e_g conduction electron spin and t_{2g} local spins. Furthermore, when the e_g electron's itinerancy is reduced, the Jahn-Teller interaction lifts the orbital degeneracy and favors the occupation of either the $d_{x^2-y^2}$ or $d_{3z^2-r^2}$ orbital on the e_g states. Essentially, the orbital degree of freedom controls the interplay between the superexchange and the double-exchange interactions, and hence has an intimate connection to the charge and spin dynamics in the doped manganites.

In recent years, the effect of the e_g orbital order (or orbital polarization) has been focused on to explain a variety of magnetic and electronic phases in the doped manganites.[3,4] The order of the e_g orbital gives rise to the anisotropy of the electron-transfer interaction. The anisotropic charge dynamics arising from such an orbital order was first observed in the dc transport for metallic $\mathrm{Nd_{0.45}Sr_{0.55}MnO_3}$ with the uniform (ferroic) order of a planar $d_{x^2-y^2}$ orbital.[5] To fully understand the orbital correlation effect of the doped manganites, including the insulating phase as well as the metallic one, the anisotropic electronic structure should be clarified by means of a spectroscopic investigation. Although a number of experimental investigations have been reported for the optical spectra of orbital ordered manganites,[6–14] most of them have neglected the existence of anisotropy in the dielectric function (optical response). This is partly because of the difficulty in preparing sufficiently size of twin-free single crystals.[5] Only a few studies of anisotropic spectra[11–14] have been reported for manganites with an e_g orbital order. Therefore, the anisotropy of electronic structure has seldom been discussed for the doped manganites with a pseudocubic perovskite structure. In this paper, we report a systematic optical study on anisotropic charge dynamics of orbital ordered manganites with various doping levels, $R_{1-x}A_x\mathrm{MnO_3}$ (R=Pr and Nd, A=Ca and Sr; $0.4 \leqslant x \leqslant 0.7$). The technical breakthrough was the successful preparation of twin-free single crystals, which enabled us to measure the detailed polarization dependence of the optical conductivity spectra. The study of polarized optical conductivity spectra is expected to clarify the role of orbital ordering in anisotropic charge dynamics of the manganite system.

To overview the spin and orbital states of the doped manganites, in Fig. 1 we display the bandwidth (W) versus hole concentration (x) phase diagram at the ground state for $R_{1-x}A_x\mathrm{MnO_3}$.[15–22] In the insets of Fig. 1 we also illustrate the schematic pictures of spin and e_g-orbital states in the respective phases. In undoped $R\mathrm{MnO_3}$ (here R=La, Pr, and Nd), $d_{3x^2-r^2}$- and $d_{3y^2-r^2}$-like orbitals for e_g electrons are alternately ordered on $\mathrm{Mn^{3+}}$ sites on the ab plane and are

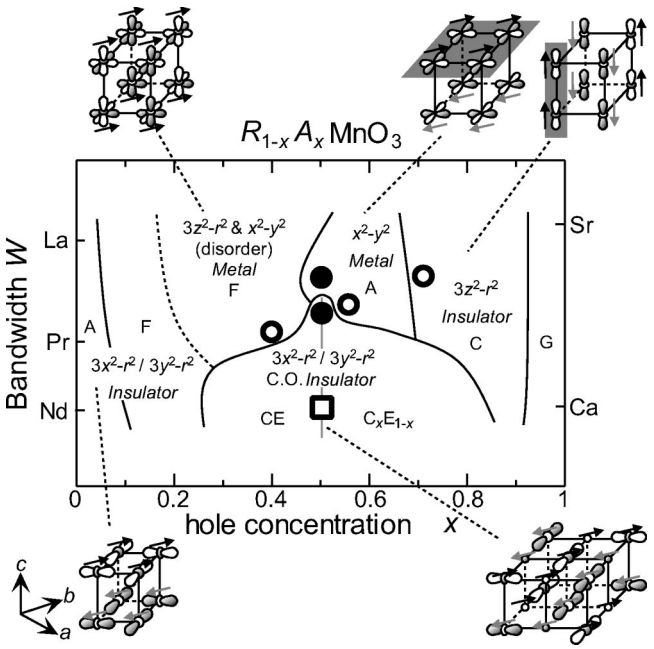

FIG. 1. Bandwidth vs hole concentration phase diagram at the ground state of $R_{1-x}A_xMnO_3$. F denotes a ferromagnetic state. A, CE, C, and G denote A-type, CE-type, C-type, and G-type antiferromagnetic states, respectively. Illustrations show schematic views of the orbital and spin configurations on Mn sites for the respective phases. The arrows represent the direction of spin. The lobes show the e_g-like orbital.

stacked parallel along the *c* axis (in the *Pbnm* orthorhombic notation), which is responsible for a layer-type (so-called A-type) antiferromagnetic (AF) order. The carrier doping induces the charge degree of freedom. When *W* is large (e.g., $La_{1-x}Sr_xMnO_3$), the ferromagnetic metallic phase with orbital quantum disorder is stabilized by maximizing the kinetic energy of the conduction e_g-like electrons for *x* between ~ 0.2 and ~ 0.5. With exceeding $x=1/2$, various magnetic and orbital ordered states appear successively; the A-type AF metallic state with uniform $d_{x^2-y^2}$ orbital order for $x\sim 0.55$, the C-type (chain-type) AF insulating state with uniform $d_{3z^2-r^2}$ orbital order for ($x\sim 0.7$), and the G-type (staggered) AF insulating state without e_g orbital. In addition to the above-mentioned sequence of magnetic and orbital ordered states, in intermediate *W* systems (e.g., $Nd_{1-x}Sr_xMnO_3$), the staggered charge ordering between Mn^{3+} and Mn^{4+} ions is realized within the *ab* plane, and is accompanied by the order of $d_{3x^2-r^2}$ and $d_{3y^2-r^2}$ orbitals at Mn^{3+} sites and the so-called CE-type (zigzag-type) AF ordering (illustrated in the lower right inset) in a narrow doping range near $x=0.5$. By contrast, in small-*W* systems such as $Nd_{1-x}Ca_xMnO_3$, the CE-type AF state appears over a wide doping range ($\sim 0.3\leqslant x\leqslant 0.5$). Furthermore, the so-called C_xE_{1-x} AF insulating state with alternate $d_{3x^2-r^2}$ and $d_{3y^2-r^2}$ orbital order is stabilized, being distinct from the systems with wide and intermediate *W* at $x>0.5$. The phase diagram of $R_{1-x}A_xMnO_3$ in Fig. 1 will be a guide map for understanding a variety of optical spectra presented in this paper.

The paper is organized as follows. Section II describes the experimental procedures. In Sec. III, we present the experimental results of optical conductivity spectra and discuss the electronic structures of doped manganites. Section III is composed of three subsections. In Sec. III A, we discuss the anisotropic spectra of charge-orbital ordered state in a half-doped manganite $Nd_{1/2}Ca_{1/2}MnO_3$. In Sec. III B. We discuss charge dynamics of double-exchange systems with varying dimensions, $Nd_{1-x}Sr_xMnO_3$ ($x=0.4$, 0.55, and 0.7). Section III C describes spectral variation affected by orbital polarization in the course of the paramagnetic-to-ferromagnetic and the ferromagnetic-antiferromagnetic transitions in $Pr_{1/2}Sr_{1/2}MnO_3$ and $Nd_{1/2}Sr_{1/2}MnO_3$. A brief summary is given in Sec. IV.

II. EXPERIMENT

A. Sample preparation

The single crystals of $R_{1-x}A_xMnO_3$ ($R=$ Pr and Nd, $A=$ Sr and Ca; $0.4\leqslant x\leqslant 0.7$) investigated here were grown by the floating-zone method. The crystal growth was performed with use of a halogen-lamp image furnace at a rate of 6–8 mm/h under an atmosphere of 1-atm O_2. The grown crystals were characterized by powder x-ray diffraction, which confirmed that the crystals have a single phase of distorted perovskite with a *Pbnm* orthorhombic or *I*4/*mcm* tetragonal structure at room temperature. The as-grown crystals have heavily twinned microstructures. To obtain twin-free crystals, we have carried out the following annealing procedure. We first oriented the crystal using Laue patterns, and cut into parallelepipeds ($\approx 3\times 3\times 2$ mm^3) with faces perpendicular to the direction of a Mn-O-Mn bond, tentatively assuming a simple cubic perovskite structure. We polished the face of the specimen with alumina powder to a mirrorlike surface for optical measurements. Then we heated the face-polished specimens to 1250 K in flowing O_2 gas, then slowly cooled down to room temperature at the cooling rate of 5 K/h. Because of the strong orthorhombicity in the orbital ordered state of $R_{1-x}A_xMnO_3$, we can visualize twinned structures with an optical microscope having crossed polarizers. In these annealed samples, the bright twin-free region has been observed to expand to millimeter size [see insets of Fig. 2(a)].

It has been pointed out that the optical conductivity spectra for some doped manganites are sensitive to residual stress of the crystal surface prepared by polishing procedure for optical measurements.[10,23] However, the above-mentioned annealing procedure plays significant roles not only in detwinning but also in removal of the residual stress. The detwinned crystals were also characterized with single-crystal x-ray diffraction measurements which confirmed the separation of the *c* axis from the *a* (or *b*) axis in the *Pbnm* orthorhombic or *I*4/*mcm* tetragonal structure.

B. Optical measurements

We performed measurements of near-normal-incidence reflectivity spectra on the (1 1 0) surface (in the *Pbnm* or *I*4/*mcm* setting) with the configurations of the electric field of incident light (*E*) parallel and perpendicular to the *c* axis. Fourier transform type spectrometers were used for the pho-

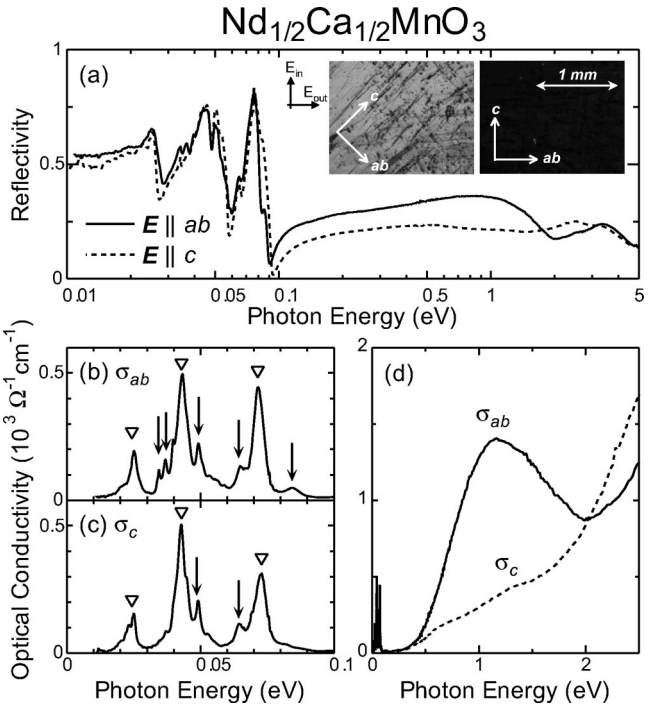

FIG. 2. Optical spectra of a detwinned crystal of $Nd_{1/2}Ca_{1/2}MnO_3$ at 10 K. (a) Reflectivity spectra for $E\|ab$ (a solid line) and $E\|c$ (a dashed line) polarization. (b) and (c) Optical conductivity spectra in the optical phonon region (0–0.08 eV). (d) Polarization dependence of the optical conductivity spectra for low-lying transitions (0–2.5 eV). The insets in (a) are polarization microscope images of a detwinned crystal of $Nd_{1/2}Ca_{1/2}MnO_3$ at 77 K (see the text).

ton energy range of 0.01–0.8 eV and grating monochromators for that of 0.6–36 eV. For the high-energy (>5 eV) measurements, we utilized the synchrotron radiation at Institute for Molecular Science as a polarized light source. The temperature dependence (10 K$\leqslant T\leqslant$700 K) of the polarized reflectivity spectra were measured for 0.01–5 eV and the room-temperature data for respective polarizations above 6 eV were connected to perform the Kramers-Kroning analysis and deduce the optical conductivity $[\sigma(\omega)]$ spectra at the respective temperatures. To prevent the reduction (oxygen loss) of the crystals, we performed the optical measurements above room temperature in flowing O_2 gas. For the analysis, we assumed the constant reflectivity below 0.01 eV and ω^{-4} extrapolation above 36 eV. Variation of the extrapolation procedures was confirmed to cause negligible difference for the calculated conductivity spectra above 0.02 eV.

III. RESULTS AND DISCUSSION

A. Anisotropic spectra of charge-orbital ordered state in $Nd_{1/2}Ca_{1/2}MnO_3$

In this section, we discuss the electronic structure of a half-doped manganite $Nd_{1/2}Ca_{1/2}MnO_3$. As shown in Fig. 1, $Nd_{1/2}Ca_{1/2}MnO_3$ has a relatively small W and shows a typical CE-type charge-orbital-spin ordering [the charge-orbital ordering temperature $T_{CO,OO}\sim 250$ K, while the Néel temperature $T_N\sim 170$ K (Refs. 24 and 25)]. First, let us overview the optical spectra at the ground state. In Fig. 2(a) we display the $T=10$ K reflectivity spectra for $E\|ab$ and $E\|c$ polarizations. An appreciable polarization dependence is readily seen in the reflectivity spectra. Spiky structures in the far-infrared region ($\hbar\omega<0.08$ eV) are due to optical phonon modes. In Figs. 2(b) and 2(c) we show the optical phonon region of the $\sigma_{ab}(\omega)$ and $\sigma_c(\omega)$ spectra, which were deduced by the Kramers-Kronig analysis of the reflectivity spectra. Three dominant peaks, commonly observed in Figs. 2(b) and 2(c) (indicated by open triangles) are the external, Mn-O bending, and Mn-O stretching phonon modes.[26] The other peaks indicated by arrows are additional phonon modes observed below $T_{CO,OO}$. These are induced by a lowering of the lattice symmetry concomitant with the charge-orbital order. Note that some of the additional modes are observed only in the $\sigma_{ab}(\omega)$ spectrum, indicating that the crystal investigated here is sufficiently detwinned with respect to the incident light polarization.

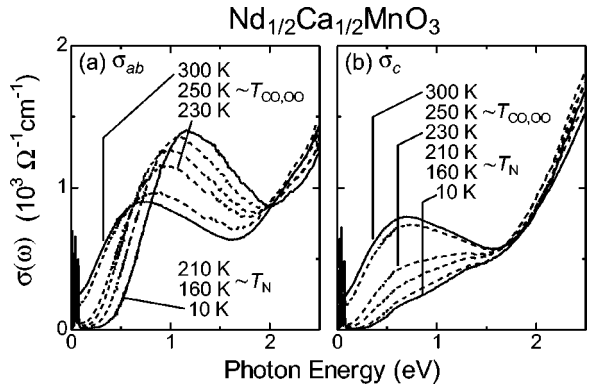

FIG. 3. Temperature dependence of the optical conductivity spectra of $Nd_{1/2}Ca_{1/2}MnO_3$ for (a) $E\|ab$ and (b) $E\perp c$ polarizations.

In Fig. 2(d) we show the polarization dependence of the $\sigma(\omega)$ spectra at 10 K for low-lying transitions. The $\sigma(\omega)$ spectra below ~ 2 eV show a huge anisotropy, reflecting the highly anisotropic electronic structure in the charge-orbital and CE-type AF ordered state. The $\sigma_{ab}(\omega)$ spectrum shows a prominent peak around 1 eV, forming a gap (≈ 0.4 eV) structure, whereas the $\sigma_c(\omega)$ spectrum has little spectral weight around 1 eV. It is worth mentioning that the anisotropy in the $\sigma(\omega)$ spectra of $Nd_{1/2}Ca_{1/2}MnO_3$ is as large as the one observed in layered manganite crystals such as single-layered $La_{1/2}Sr_{3/2}MnO_4$ (Ref. 27) or bilayered $La_{2-2x}Sr_{1+2x}Mn_2O_7$.[28]

The T evolution of the $\sigma_{ab}(\omega)$ and $\sigma_c(\omega)$ spectra for the $Nd_{1/2}Ca_{1/2}MnO_3$ is shown in Fig. 3. As for the $\sigma_{ab}(\omega)$ spectra [Fig. 3(a)], the peak structure is gradually suppressed and shifted to the lower energy region with the increase of T. The gap structure that exists in the low-$T\sigma_{ab}(\omega)$ spectra gradually diminishes at high T, while forming a pseudogap structure with a nonzero $\sigma_{ab}(\omega=0)$ value. As for the $\sigma_c(\omega)$ spectra, by contrast, the low-energy (<1.5 eV) spectral weight, that is suppressed at low T, tends to increase with the increase of T. At $T\geqslant T_{CO,OO}$, the spectra show a nearly polarization-independent shape with a broad peak around 0.7 eV. This is distinct from the spectra of layered manganites

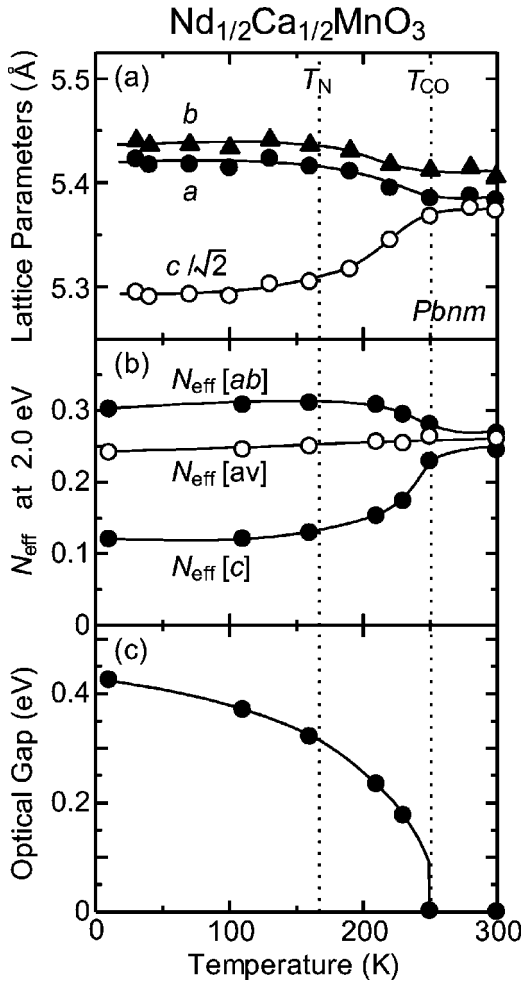

FIG. 4. (a) Temperature profiles of the lattice parameters of $Nd_{1/2}Ca_{1/2}MnO_3$. (b) Temperature dependence of the effective number of electrons N_{eff} for the $E\|ab$ and $E\|c$ polarizations which are deduced by integrating the observed $\sigma(\omega)$ spectra over the region, 0 eV$\leqslant\omega\leqslant$2.0 eV. $N_{\mathrm{eff}}[\mathrm{av}]$ denotes the averaged spectral weight defined by $N_{\mathrm{eff}}[\mathrm{av}]=(2N_{\mathrm{eff}}[ab]+N_{\mathrm{eff}}[c])/3$. (c) Temperature dependence of the optical gap magnitude as estimated by linearly extrapolating the rising part of the optical conductivity spectra for $E\|ab$. Solid lines are merely guides to the eyes.

such as $La_{1/2}Sr_{3/2}MnO_4$, in which remarkable anisotropy remains even above $T_{\mathrm{CO,OO}}$.[29] It is noteworthy that a discontinuous spectral change from pseudo-gap to real-gap like structures is discernible in Fig. 3 at $T_{\mathrm{CO,OO}}$, while no remarkable change in the spectra takes place around T_{N}.

To evaluate the T dependence of the spectral weight, we use the effective number of electrons $N_{\mathrm{eff}}(\omega)$, as defined by the following relation:

$$N_{\mathrm{eff}}(\omega)=\frac{2m}{\pi e^2 N}\int_0^{\omega}\sigma(\omega')d\omega'. \tag{1}$$

Here, N represents the number of formula units (i.e., the number of Mn atoms per unit volume). We plot the $N_{\mathrm{eff}}[ab]$ and $N_{\mathrm{eff}}[c]$ values in Fig. 4(b) as a function of T, adopting a cutoff energy at $\hbar\omega=2.0$ eV, below which most of the T-dependent spectral change occurs. At 10 K. $N_{\mathrm{eff}}[ab]$ is more than twice as large as the $N_{\mathrm{eff}}[c]$, showing a clear anisotropic feature. In the mid-T region, $T_{\mathrm{N}}<T<T_{\mathrm{CO,OO}}$, $N_{\mathrm{eff}}[ab]$ decreases while $N_{\mathrm{eff}}[c]$ increases with the increase of T, leading to the decrease of the anisotropy. The T dependence of N_{eff} appears to be related to that of the lattice parameters [Fig. 4(a)] which is tied to the orbital state via the collective Jahn-Teller effect. This result clearly indicates the strong relationship between the spectral anisotropy and the formation of the orbital ordering. We also estimated the onset energy of the peak structure in the $\sigma_{ab}(\omega)$ spectra by extrapolating linearly the rising part to the abscissa. Figure 4(c) displays the T profile of the onset energy for $\sigma_{ab}(\omega)$ spectra as a measure of the optical gap energy. At the lowest T ($=10$ K), the gap magnitude is approximately 0.4 eV, and gradually decreases as T is increased (e.g., 0.18 eV at 230 K), and then is suppressed abruptly to zero at $T_{\mathrm{CO,OO}}$. These results demonstrate that the onset of the long-range CE-type AF order scarcely induces the abrupt change in the anisotropic electronic structure below 2 eV and the gap magnitude, while the charge-orbital order plays a major role in determining them. In Fig. 4(b) we also show the averaged spectral weight $N_{\mathrm{eff}}[\mathrm{av}]=(2N_{\mathrm{eff}}[ab]+N_{\mathrm{eff}}[c])/3$ at 2.0 eV, as a measure of the total spectral weight below 2 eV. In spite of the remarkable T dependence in $\sigma_{ab}(\omega)$ and $\sigma_c(\omega)$, $N_{\mathrm{eff}}[\mathrm{av}]$ is nearly T independent, which indicates that the total kinetic energy measured on an energy scale of 2.0 eV is preserved during the charge-orbital order (and CE-type AF) transitions.

There have been reported several theoretical studies on the optical properties of the charge-orbital ordered manganites. Solovyev[30] interpreted the optical conductivity in the CE-type AF phase to dipole transitions from Mn(e_g) to Mn($4p$) states by means of tight-binding approaches and first principles band-structure calculations in the local spin-density approximation. To reproduce the experimental results such as large optical gap and anisotropy, the effect of the Jahn-Teller distortion and the zigzag-type (i.e., CE-type) AF ordering are indispensable in his calculation. This means that the calculation may explain the optical conductivity spectra at the ground state but hardly reproduce those at $T_{\mathrm{N}}\leqslant T\leqslant T_{\mathrm{CO,OO}}$ where the magnetic ordering disappears. More recently, Cuoco *et al.*[31] studied the model for the CE phase, which includes on-site and intersite Coulomb interactions as well as the Jahn-Teller orbital polarization by the exact diagonalization method. They investigated the nature of the optical excitation as due to transitions between the correlated states of e_g electrons at Mn^{3+} sites, and explained the pseudogap feature in a high T region as observed experimentally.

The undoped $R\mathrm{MnO_3}$ is classified as a charge-transfer type insulator located near the boundary of a Mott type insulator.[32,33] In doped manganites, therefore, the hybridized O $2p$–Mn e_g state may form a conduction band and the intraband and interband transitions of the hybridized states dominate the lower-lying electronic excitations in doped manganites. The spectra below $\sim$2 eV investigated here should reflect such O $2p$–Mn e_g hybridized bands. The observed anisotropy of the $\sigma(\omega)$ spectra indicates that the ki-

netic energy of conduction electrons measured on this energy scale (~ 2 eV) is suppressed for the component along the c axis at the ground state. In the framework of the intersite d-d transition model, the peak structure in the $\sigma(\omega)$ spectrum can be assigned to the photoinduced hopping of the e_g electron between Mn^{3+} and Mn^{4+} sites, whose anisotropy can be interpreted in terms of the (a) charge, (b) orbital, and (c) spin orders as follows. (a) The charge stacking along the c axis prohibits the hopping to the c direction by the strong on-site Coulomb repulsion. (b) The spectral weight depends on the electron transfer energy, and hence becomes anisotropic in the $d_{3x^2-r^2}/d_{3y^2-r^2}$-type orbital ordered state [stronger for $\sigma_{ab}(\omega)$ than $\sigma_c(\omega)$]. (c) Since the total spin quantum number is preserved during the optical excitation, intersite transitions along the c axis between AF-coupled Mn sites should be forbidden by the large Hund's-rule coupling energy. All of them may be relevant to the observed anisotropy in the optical spectra to some extent: Mechanisms (a) and (b) simultaneously work for the suppression of the c-polarized spectral weight since the charge and orbital orders occur concomitantly. Mechanism (c) is effective even in the case of short-range correlation, and hence may be also responsible for the decrease of $N_{\rm eff}[c]/N_{\rm eff}[ab]$ [Fig. 4(b)] above $T_{\rm N}$.

B. Charge dynamics in an anisotropic double-exchange system, $Nd_{1-x}Sr_xMnO_3$ ($x=0.4$, 0.55, and 0.7)

In this section, we discuss the optical spectra of $Nd_{1-x}Sr_xMnO_3$ ($x=0.4$, 0.55, and 0.7) with controlled band fillings (doping levels). We begin with the features at the ground state. As shown in Fig. 1, the orbital and spin structures for $Nd_{1-x}Sr_xMnO_3$ are summarized as follows: the ferromagnetic-metallic state with no (long-range) orbital order ($T_{\rm C}\approx 270$ K) for $x=0.4$, the layer-type (A-type) AF state with $d_{x^2-y^2}$ orbital order ($T_{\rm N}\approx 240$ K) for $x=0.55$, and the chain-type (C-type) AF state with $d_{3z^2-r^2}$ orbital order ($T_{\rm N}\approx 270$ K) for $x=0.7$. The ferromagnetic spin arrangement with spatials extents of three dimensional (3D) ($x=0.4$), 2D ($x=0.55$), and 1D ($x=0.7$) is all due to the double-exchange (DE) interaction. In other words, the increase of x gives rise to the reduction of the dimensionality of the DE ferromagnetic interaction.[3] Figure 5 shows the $T=10$ K $\sigma(\omega)$ spectra for $Nd_{1-x}Sr_xMnO_3$ ($x=0.4$, 0.55, and 0.7). In the figure, solid and dashed lines denote the $\sigma(\omega)$ spectra with E parallel [$\sigma_{\|}(\omega)$] and perpendicular [$\sigma_{\perp}(\omega)$] to the ferromagnetically coupled Mn sites (see and compare the right insets of Fig. 5). For $x=0.4$ with ferromagnetic-metallic orbital-disordered state, the $\sigma(\omega)$ forms a Drude-like peak centered at $\omega=0$, which reflects the coherent motion of charge carriers. [Here, we used the terms ''Drude-like'' and ''coherent'' for the shape of $\sigma(\omega)$ with a peak centered at $\omega=0$, although the whole infrared spectral shape of the $x=0.4$ compound, whose broad tail of conductivity persists up to ≈ 1 eV, cannot be described with the conventional Drude form alone.[34,35]] In the $x=0.55$ and 0.7 crystals, $\sigma(\omega)$ spectra show a remarkable polarization dependence, reflecting the highly anisotropic electronic structure in the spin- and orbital-ordered state, as illustrated in the right insets of Fig. 5. The details of the T dependence of the spectral anisotropy for $x=0.55$ and 0.7 have been reported elsewhere.[14] Here, we focus on another noteworthy feature, i.e., the evolution of the gap structure with reducing dimensionality of the DE interaction, from the Drude-like coherent peak for $x=0.4$ to a *pseudo*gap for $x=0.55$ and then to a *real* gap for $x=0.7$. [Here the pseudogap means the peaked spectral feature with an appreciable $\sigma(\omega>0)$ value but with no Drude peak.] This signals an extremely diffuse charge dynamics within ferromagnetic two-dimensional sheets and one-dimensional chains.

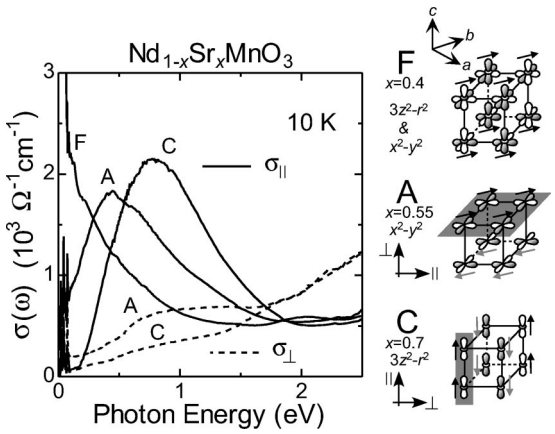

FIG. 5. Polarization dependence of the optical conductivity spectra at 10 K for $x=0.4$, 0.55, and $x=0.7$ crystals. Illustrations show schematic views of the orbital and spin configurations.

In the following, we discuss the relationship between the charge dynamics and the dimensionality of spin/orbital structure on the basis of the x- and T-dependent spectra for $Nd_{1-x}Sr_xMnO_3$. The T variation of the $\sigma_{\|}(\omega)$ spectra for the respective doping levels is shown in Figs. 6(a)–6(c). In each case, a conspicuous spectral weight transfer is observed over a wide energy range (>2 eV). With the increase of T from 10 K, the low-energy spectral weight is gradually suppressed, and some part is transferred to a higher energy region ($\omega>0.7$ eV for $x=0.4$, and $\omega>1.5$ eV for $x=0.55$ and 0.7). The gap structure, which exists in the low-T $\sigma_{\|}(\omega)$ spectra for the $x=0.7$ compound, gradually diminishes with the increase of T. At high T, the spectra show a nearly x-independent shape with a broad peak structure for the respective compounds.

To evaluate the spectral variation quantitatively, we calculated $N_{\rm eff}[\|]$ as defined by Eq. (1). Figure 6(d) shows the $N_{\rm eff}[\|]$ at 0.1 eV, as a measure of the coherent component of the $\sigma_{\|}(\omega)$ spectra. The $N_{\rm eff}[\|]$ ($\omega_{\rm c}=0.1$ eV) values are distinct for the respective compounds in the low-T spin ordered phase, but nearly converge to a comparable value ($\sim 10^{-2}$) in the high-T paramagnetic phase. This indicates that the effect of the spin order on the coherent motion of e_g electrons, that is closely related to the dc transport, strongly depends on the spin and orbital structure. We also show the $N_{\rm eff}[\|]$ at 2.0 eV in Fig. 6(e). The overall features of $N_{\rm eff}[\|]$ at 2.0 eV [Fig. 6(e)] rather resemble each other for the respective compositions, although the T variation of $N_{\rm eff}[\|]$ for $x=0.55$ and 0.7 persists up to much higher T than $T_{\rm N}$. These

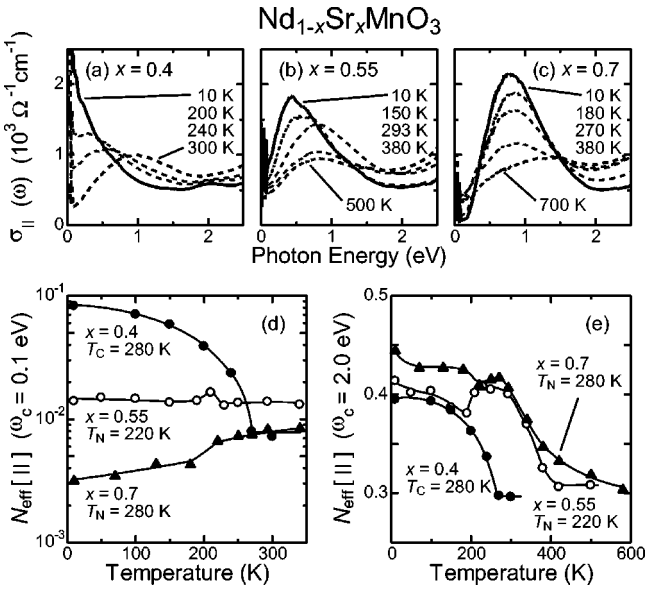

FIG. 6. (a)–(c) Temperature dependence of optical conductivity spectra with the light polarization along the ferromagnetic direction for $Nd_{1-x}Sr_xMnO_3$ [(a) $x=0.4$, (b) $x=0.55$, and (c) $x=0.7$]. (d), and (e) Temperature dependence of the effective number of electrons N_{eff} for the respective polarizations, deduced by integrating the observed $\sigma(\omega)_{\parallel}$ spectra ($0\leqslant\omega\leqslant\omega_c$) of $Nd_{1-x}Sr_xMnO_3$ ($x=0.4$, 0.55, and 0.7) [(d) $\omega_c=0.1$ eV and (e) $\omega_c=2.0$ eV]. Solid lines in (d) and (e) are merely guides to the eyes.

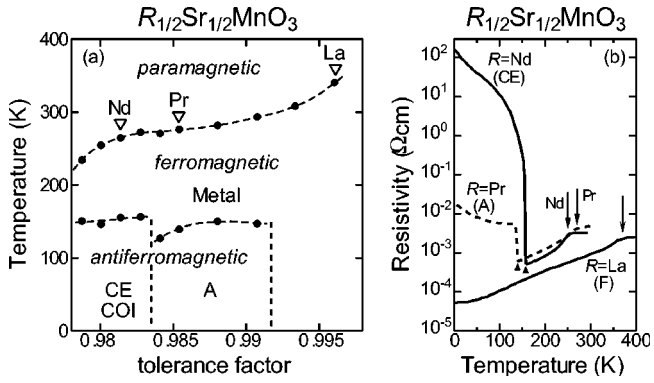

FIG. 7. (a) Magnetic and electronic phase diagram of $R_{1/2}Sr_{1/2}MnO_3$. Broken lines are merely guides to the eyes. (b) Temperature dependence of resistivity for $R_{1/2}Sr_{1/2}MnO_3$ ($R=$La, Pr, and Nd) crystals. Arrows denote the T_C (Curie temperature) for the respective compounds. Closed triangles indicate the T_N (Néel temperature) for $R=$Pr and Nd crystals.

results represent that the kinetic energy of conduction electrons scarcely changes when measured on a large ($\sim$2 eV) energy, whereas the coherent motion as measured on a low-energy scale is critically suppressed with a reduced dimensionality of DE interaction. One of the plausible scenarios for the x dependence of $\sigma_{\parallel}(\omega)$ is that electron correlation such as short-range charge order (and its coupling with lattice dynamics) is enhanced by the increased low-dimensional nature of spin and orbital order. The formation of short-range charge ordering at the A-type AF and/or $d_{x^2-y^2}$-type orbital ordered phase was indicated by the structural modulation observed by neutron diffraction measurements[36] as well as angle-resolved photoemission spectroscopy,[37] in which a Fermi surface nesting corresponding to the structural modulation[38] was observed. The tendency of charge ordering at the A-type AF and $d_{x^2-y^2}$-type orbital ordered phase has also been suggested theoretically. Mizokawa and Fujimori[39] proposed, on the basis of Hartree-Fock calculations, that the A-type spin ordering in a half-doped manganite is accompanied by a checkerboard-type charge ordering of Mn^{3+} and Mn^{4+}. Mack and Horsch[40] calculated the $d_{x^2-y^2}$ orbital correlation between the nearest neighbor sites in the ferroic $d_{x^2-y^2}$ orbital ordered state, and suggested the tendency of the charge ordering.

C. Spectral variation with antiferromagnetic-ferromagnetic and ferromagnetic-paramagnetic transitions in $Pr_{1/2}Sr_{1/2}MnO_3$ and $Nd_{1/2}Sr_{1/2}MnO_3$

In this section, we discuss the anisotropic orbital correlation in the ferromagnetic-metallic phase in terms of the optical spectra of half-doped manganite crystals $Pr_{1/2}Sr_{1/2}MnO_3$ and $Nd_{1/2}Sr_{1/2}MnO_3$. In the vicinity of the doping level $x=0.5$, the ferromagnetic metallic, A-type AF metallic, and charge-ordered CE-type AF insulating phases compete strongly with each other, and the phase diagram becomes complicated, as seen in Fig. 1. This multicritical feature is closely tied with dramatic phase conversions attained in doped manganites such as the CMR effect. Figure 7(a) shows the magnetic/electronic phase diagram of $R_{1/2}Sr_{1/2}MnO_3$ as a function of the tolerance factor f,[41] which is taken from Ref. 42. In the large-f region, say $La_{1/2}Sr_{1/2}MnO_3$, the ground state is the ferromagnetic and the dc resistivity shows a metallic feature below T_C [Fig. 7(b)]. With decreasing f, the ground state successively changes to the A- and CE-type AF phases. For example, $Pr_{1/2}Sr_{1/2}MnO_3$ has the A-type AF phase with the $d_{x^2-y^2}$-type orbital order, while $Nd_{1/2}Sr_{1/2}MnO_3$ has the CE-type AF phase with the charge-orbital order (also see Fig. 1). In $Pr_{1/2}Sr_{1/2}MnO_3$ and $Nd_{1/2}Sr_{1/2}MnO_3$, the following successive magnetic phase transitions take place with increasing T from the ground state: the antiferromagnetic (AF) $\rightarrow$ ferromagnetic (F) $\rightarrow$ paramagnetic (P) phase. These magnetic transitions are accompanied by remarkable changes in the dc resistivity as shown in Fig. 7(b).

In Figs. 8 and 9 we show the polarized reflectivity and $\sigma(\omega)$ spectra for the AF, F, and P phases of $Pr_{1/2}Sr_{1/2}MnO_3$ and $Nd_{1/2}Sr_{1/2}MnO_3$. First, let us focus on the spectral variation with the successive magnetic transitions in $Pr_{1/2}Sr_{1/2}MnO_3$. At a glance, one may notice a conspicuous polarization dependence for the respective phases. The $\sigma_{\parallel}(\omega)$ spectrum at the A-type AF phase (10 K) shows a broad peak around 0.5 eV with a *pseudo*gap structure, having a much larger spectral weight than the $\sigma_{\perp}(\omega)$ spectrum. These features bear a close resemblance to those of $Nd_{1-x}Sr_xMnO_3$ ($x=0.55$) (see Fig. 5 and Ref. 14) with the same type of the spin (A-type) and orbital ($d_{x^2-y^2}$-type) order pattern [the inset of Fig. 8(d)]. In the F phase (150 K), the broad peak around 0.5 eV is suppressed and is shifted toward lower energy. Then, the $\sigma_{\parallel}(\omega\sim0)$ is increased. With

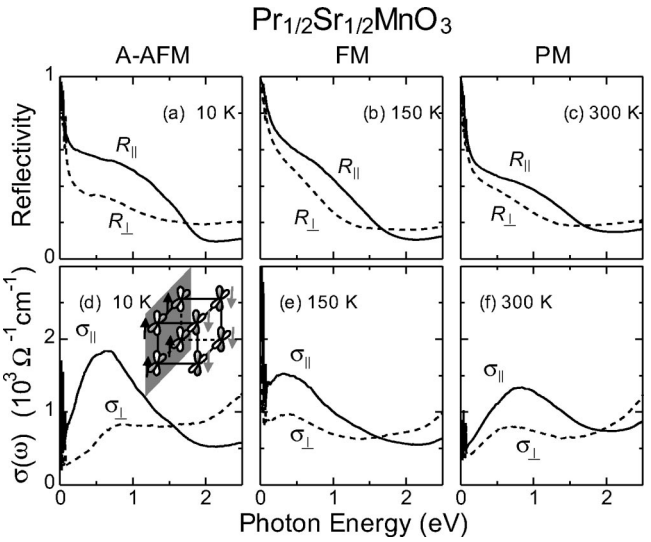

FIG. 8. Optical reflectivity [(a)–(c)] and conductivity [(d)–(f)] spectra of a detwinned crystal of $Pr_{1/2}Sr_{1/2}MnO_3$ at representative temperatures; (a) and (d) 10 K ($T<T_N$), (b) and (e) 150 K ($T_N<T\ll T_C$), and (c) and (f) 300 K ($T>T_C$).

a further increase of T, the peak in $\sigma_{\|}(\omega)$ again shifts to higher energy, although the peak height decreases. The T-variation of the spectra is well in accord with that of the dc resistivity.

To further clarify the T dependence of the low-energy spectral weight, we plot the $N_{\mathrm{eff}}[\|]$ and $N_{\mathrm{eff}}[\perp]$ values in Fig. 10(a) as a function of T, adopting the cutoff energy of 0.5 eV. At the A-type AF phase, a remarkable anisotropy can be seen in N_{eff}, and $N_{\mathrm{eff}}[\|]$ and $N_{\mathrm{eff}}[\perp]$ are both nearly T independent. At T_N, the $N_{\mathrm{eff}}[\|,\perp]$ are discontinuously increased but their anisotropy still remains even above T_N. Further increasing T toward T_C, N_{eff} gradually decreases. Nevertheless, the anisotropy of N_{eff} appears to subsist above

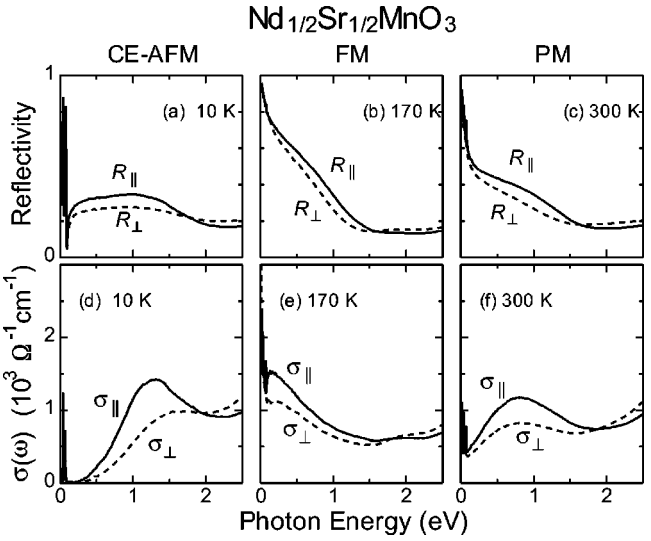

FIG. 9. Optical reflectivity [(a)–(c)] and conductivity [(d)–(f)] spectra of a detwinned crystal of $Nd_{1/2}Sr_{1/2}MnO_3$ at representative temperatures; (a) and (d) 10 K ($T<T_N$), (b) and (e) 150 K ($T_N<T\ll T_C$), and (c) and (f) 300 K ($T>T_C$).

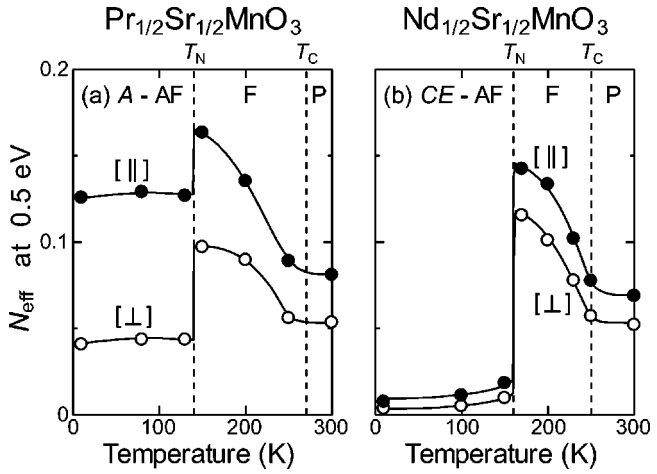

FIG. 10. Temperature dependence of the effective number of electrons N_{eff} of (a) $Pr_{1/2}Sr_{1/2}MnO_3$ and (b) $Nd_{1/2}Sr_{1/2}MnO_3$ for the respective polarizations, deduced by integrating the observed $\sigma(\omega)_{\|}$ and $\sigma(\omega)_{\perp}$ spectra (0 eV$\leqslant\hbar\omega\leqslant$0.5 eV). Solid lines are merely guides to the eyes. A-AF, CE-AF, F, and P stand for A-type antiferromagnetic and CE-type antiferromagnetic, ferromagnetic, and paramagnetic phases, respectively.

T_C. The most striking is that the anisotropy is also evident even in the ferromagnetic-metallic phase (150 K). This is in contrast to the ordinary F state of the manganite. Typical DE ferromagnetic-metallic phases in doped manganites are accompanied by orbital (quantum) disordering, which makes their electronic structure nearly isotropic. Such an anisotropy of the electronic structure in the F state manifests itself in the spin-wave dispersion relation. For example, the isotropic spin-wave dispersion relation, e.g., irrespective along the $[hh\,0]$ and $[0\,0\,l]$ directions, has been reported for the ferromagnetic-metallic phase in $La_{1-x}Sr_xMnO_3$ ($0.12\leqslant x\leqslant 0.3$).[43] More recently, however, a strong anisotropy in the spin wave excitations has been observed in the mid-T F metallic region of $Pr_{1/2}Sr_{1/2}MnO_3$ by Yoshizawa and co-workers.[44,45] They inferred from the anisotropic spin-wave dispersion that the $d_{x^2-y^2}$-type orbital ordering which is identical with that in the low-T phase persists in the intermediate F phase, and causes a strong anisotropy in the spin dynamics. If we follow their interpretation, the stronger spectral weight of $\sigma(\omega)$ spectra in our results is attributable to the stronger DE interaction caused by the $d_{x^2-y^2}$-type orbital ordering. However, the observed anisotropic spectra at the P phase is rather similar to that in $Nd_{1-x}Sr_xMnO_3$ ($x=0.55$), in which the directional order of $d_{3x^2-r^2}$-like (rod-type) e_g orbital seems to persist far above T_N.[14] Furthermore, the crystal structure at the respective phases in $Pr_{1/2}Sr_{1/2}MnO_3$ are still under controversy[18,19,46,47] at the present stage.[48] With respect to the possible pattern of the orbital polarization or correlation, therefore, there is also another option that the directional order of rod-type $d_{3x^2-r^2}$-like e_g orbital exists in the F and P phases through the switching of the orbital ordering pattern at T_N ($d_{x^2-y^2}$-type $\leftrightarrow d_{3x^2-r^2}$-type). In this case, the observed anisotropic optical spectra in the F and P phases should be due to the rod-type orbital ordering. In any case, a remarkable

change in the crystal structure occurs only at T_N, not at T_C, suggesting the occurrence of the same orbital ordering pattern at the F and P phases. It should be noted that the spectral weight is shifted toward low energy by the ferromagnetic ordering, which clearly indicates that the three-dimensional development of the DE ferromagnetic interaction makes the charge dynamics more coherent even in the orbital ordered phase.

Let us turn to the optical spectra of $Nd_{1/2}Sr_{1/2}MnO_3$ (Fig. 9). In all three phases, the spectra show an anisotropy as in $Pr_{1/2}Sr_{1/2}MnO_3$. However, one significant difference appears in the low-T AF phase because of the different patterns of orbital and spin order. As shown in Fig. 9(d), a clear real gap with an onset around 0.4 eV is observed at 10 K. This gap feature is similar to that in $Nd_{1/2}Ca_{1/2}MnO_3$ (Fig. 3), and can be attributed to the Mn^{3+}-Mn^{4+} charge ordering accompanied by the ordering of the alternate $d_{3x^2-r^2}/d_{3y^2-r^2}$-type orbital and CE-type spin. At the F and P phases, the spectral shapes are similar to those in $Pr_{1/2}Sr_{1/2}MnO_3$, although the magnitude of anisotropy is smaller.[49] These differences and similarities in spectral feature between $Nd_{1/2}Sr_{1/2}MnO_3$ and $Pr_{1/2}Sr_{1/2}MnO_3$ are also manifested in the T profiles of N_{eff} (see Fig. 10).

An anisotropic spin-wave dispersion relation has also been observed in the F phase of $Nd_{1/2}Sr_{1/2}MnO_3$,[44,45] which may be closely related to the observed anisotropy in optical spectra as in $Pr_{1/2}Sr_{1/2}MnO_3$. Furthermore, the smaller magnitude of the optical anisotropy in $Nd_{1/2}Sr_{1/2}MnO_3$ than that in $Pr_{1/2}Sr_{1/2}MnO_3$ qualitatively coincides with a similar tendency of the anisotropy in the spin-wave dispersion. All the observations in this section clearly point to the existence of a directional order of the orbital persisting even in the F metallic phase of $Pr_{1/2}Sr_{1/2}MnO_3$ and $Nd_{1/2}Sr_{1/2}MnO_3$.

There are several microscopic observations which suggest the existence of a spatially fine mixture of charge-ordered and ferromagnetic-metallic phases in the vicinity of T_N for $Nd_{1/2}Sr_{1/2}MnO_3$.[50,51] In addition, based on the observation of diffuse streaks in electron diffraction patterns, Fukumoto *et al.* insisted that the charge-ordered phases exist as microdomains even far above T_N in the F phase.[50] If charge-ordered microdomains exist in the F phase and affect the optical spectra, their contribution to the spectra may monotonically increase with decreasing temperature from T_C to T_N, because, in terms of electronic phase separation, the charge-ordered region may expand as temperature approaches T_N. As shown in Fig. 10, however, N_{eff} ($\omega_c = 0.5$ eV) monotonically increases with decreasing temperature in the F phase. This suggests that the charge-ordered region with a real-gap structure is not significantly reflected in the spectra or does not exist in the F phase of the stress-free single crystals investigated here.

IV. SUMMARY

We have investigated the polarization and temperature dependence of the optical conductivity spectra in various orbital ordered phases for detwinned single crystals of doped perovskite manganites $R_{1-x}A_xMnO_3$ (R=Pr and Nd, A=Ca and Sr; $0.4 \leqslant x \leqslant 0.7$). The present study has revealed that the electronic structures of heavily hole-doped manganites show a remarkable anisotropy due to the order of e_g-like orbitals in spite of their pseudocubic lattice structure. The orbital polarization causes anisotropic interaction (e.g. superexchange and double-exchange interactions), and then gives rise to the low-dimensional spin structure such as the layered-type, the chain-type, and zigzag-type antiferromagnetic orderings. In such antiferromagnetic ground states, the large anisotropy is present in optical conductivity spectra with respect to light polarization. Surprisingly, we have also observed a substantial optical anisotropy even in some ferromagnetic phases adjacent to the orbital-ordered antiferromagnetic phase. This is indicative of the existence of the orbital-polarized ferromagnetic phase in some doped manganites such as $Pr_{1/2}Sr_{1/2}MnO_3$ and $Nd_{1/2}Sr_{1/2}MnO_3$.

ACKNOWLEDGMENTS

We thank Y. Okimoto, E. Saitoh, and R. Kajimoto for fruitful discussions. This work was supported in part by the New Energy and Industrial Technology Development Organization (NEDO) and Grant-in-Aid for Scientific Research Priority Area from the Ministry of Education, Culture, Sports, Science, and Technology of Japan.

*Present address: Los Alamos National Laboratory, Los Alamos, New Mexico 87545, USA.

[1] For a review, see for example, *Colossal Magnetoresistive Oxides*, edited by Y. Tokura (Gordon & Breach, Tokyo, 1999).
[2] For a review, see for example, E. Dagotto, T. Hotta, and A. Moreo, Phys. Rep. **344**, 1 (2001).
[3] R. Maezono, S. Ishihara, and N. Nagaosa, Phys. Rev. B **57**, R13993 (1996); **58**, 11 583 (1998).
[4] Y. Tokura and N. Nagaosa, Science **288**, 462 (2000).
[5] H. Kuwahara, T. Okuda, Y. Tomioka, A. Asamitsu, and Y. Tokura, Phys. Rev. Lett. **82**, 4316 (1999).
[6] H.L. Liu, S.L. Cooper, and S-W. Cheong, Phys. Rev. Lett. **81**, 4684 (1998).
[7] J.H. Jung, H.J. Lee, T.W. Noh, E.J. Choi, Y. Moritomo, Y.J. Wang, and X. Wei, Phys. Rev. B **62**, 481 (2000).
[8] Y. Okimoto, Y. Konishi, M. Izumi, T. Manako, M. Kawasaki, and Y. Tokura, J. Phys. Soc. Jpn. **71**, 613 (2002).
[9] K.H. Kim, S. Lee, T.W. Noh, and S.-W. Cheong, Phys. Rev. Lett. **88**, 167204 (2002).
[10] K. Takenaka, S. Okuyama, S. Sugai, and M.Y. Maksimuk, J. Phys. Soc. Jpn. **71**, 3065 (2002).
[11] Y. Okimoto, Y. Tomioka, Y. Onose, Y. Otsuka, and Y. Tokura, Phys. Rev. B **57**, R9377 (1998); **59**, 7401 (1999).
[12] M. Rübhausen, S. Yoon, S.L. Cooper, K.H. Kim, and S-W. Cheong, Phys. Rev. B **62**, R4782 (2000).
[13] M.W. Kim, J.H. Jung, K.H. Kim, H.J. Lee, J. Yu, T.W. Noh, and Y. Moritomo, Phys. Rev. Lett. **89**, 016403 (2002).
[14] K. Tobe, T. Kimura, and Y. Tokura, Phys. Rev. B **67**, 140402(R) (2003).
[15] E.O. Wollan and W.C. Koehler, Phys. Rev. **100**, 545 (1955).
[16] J.B. Goodenough, Phys. Rev. **100**, 564 (1955).
[17] Z. Jirák, S. Krupicka, Z. Simsa, M. Dlouhá, and S. Vratislav, J.

Magn. Magn. Mater. **53**, 153 (1985).
[18] K. Knízek, Z. Jírak, E. Pollert, and F. Zounová, J. Solid State Chem. **100**, 292 (1992).
[19] H. Kawano, R. Kajimoto, H. Yoshizawa, Y. Tomioka, H. Kuwahara, and Y. Tokura, Phys. Rev. Lett. **78**, 4253 (1997).
[20] T. Akimoto, Y. Maruyama, Y. Moritomo, A. Nakamura, K. Hirota, K. Ohoyama, and M. Ohashi, Phys. Rev. B **57**, R5594 (1998).
[21] R. Kajimoto, H. Yoshizawa, H. Kawano, H. Kuwahara, Y. Tokura, K. Ohoyama, and M. Ohashi, Phys. Rev. B **60**, 9506 (1999).
[22] P.G. Radaelli, D.E. Cox, L. Capogna, S.-W. Cheong, and M. Marezio, Phys. Rev. B **59**, 14 440 (1999).
[23] K. Takenaka, K. Iida, Y. Sawaki, S. Sugai, Y. Moritomo, and A. Nakamura, J. Phys. Soc. Jpn. **68**, 1828 (1999).
[24] K. Liu, X.W. Wu, K.H. Ahn, T. Sulchek, C.L. Chien, and J.Q. Xiao, Phys. Rev. B **54**, 3007 (1996).
[25] T. Vogt, A.K. Cheetham, R. Mahendiran, A.K. Raychaudhuri, R. Mahesh, and C.N.R. Rao, Phys. Rev. B **54**, 15 303 (1996).
[26] S. Tajima, A. Masaki, S. Uchida, T. Matsuura, K. Fueki, and S. Sugai, J. Phys. C **20**, 3469 (1987).
[27] T. Ishikawa, K. Ookura, and Y. Tokura, Phys. Rev. B **59**, 8367 (1999).
[28] T. Ishikawa, K. Tobe, T. Kimura, T. Katsufuji, and Y. Tokura, Phys. Rev. B **62**, 12 354 (2000).
[29] J.H. Jung, J.S. Ahn, J.J. Yu, T.W. Noh, J.H. Lee, Y. Moritomo, I. Solovyev, and K. Terakura, Phys. Rev. B **61**, 6902 (2000).
[30] I.V. Solovyev, Phys. Rev. B **63**, 174406 (2001).
[31] M. Cuoco, C. Noce, and A.M. Oleś, Phys. Rev. B **66**, 094427 (2002).
[32] J. Zaanen, G.A. Sawatzky, and J.W. Allen, Phys. Rev. Lett. **55**, 418 (1985).
[33] T. Arima, Y. Tokura, and J.B. Torrance, Phys. Rev. B **48**, 17 006 (1993); T. Arima and Y. Tokura, J. Phys. Soc. Jpn. **64**, 2488 (1995).
[34] S. Ishihara, M. Yamanaka, and N. Nagaosa, Phys. Rev. B **56**, 686 (1997).
[35] P. Horsch, J. Jaklic, and F. Mack, Phys. Rev. B **59**, 6217 (1999).
[36] R. Kajimoto, H. Yoshizawa, Y. Tomioka, and Y. Tokura, Phys. Rev. B **66**, 180402(R) (2002).
[37] Y.-D. Chuang, A.D. Gromko, D.S. Dessau, T. Kimura, and Y. Tokura, Science **292**, 1509 (2001).
[38] B.J. Campbell, R. Osborn, D.N. Argyriou, L. Vasiliu-Doloc, J.F. Mitchell, S.K. Sinha, U. Ruett, C.D. Ling, Z. Islam, and J.W. Lynn, Phys. Rev. **65**, 014427 (2002).
[39] T. Mizokawa and A. Fujimori, Phys. Rev. B **56**, R493 (1997).
[40] F. Mack and P. Horsch, Phys. Rev. Lett. **82**, 3160 (1999).
[41] The tolerance factor f is defined as $f=(\langle r_A\rangle+r_O)/[\sqrt{2}(r_{Mn}+r_O)]$, where $\langle r_A\rangle$, r_{Mn}, and r_O are (average) ionic radii of the respective sites.
[42] H. Kuwahara, Y. Moritomo, Y. Tomioka, A. Asanitsu, M. Kasai, and Y. Tokura, J. Appl. Phys. **81**, 4954 (1997).
[43] K. Hirota, N. Kaneko, A. Nishizawa, Y. Endoh, M.C. Martin, and G. Shirane, Physica C **237-238**, 36 (1997).
[44] H. Yoshizawa, R. Kajimoto, H. Kawano, J.A. Fernandez-Baca, Y. Tomioka, H. Kuwahara, and Y. Tokura, Mater. Sci. Eng., B **63**, 125 (1999).
[45] H. Kawano-Furukawa, R. Kajimoto, H. Yoshizawa, Y. Tomioka, H. Kuwahara, and Y. Tokura, Phys. Rev. B **67**, 174422 (2003).
[46] D.N. Argyriou, D.G. Hinks, J.F. Mitchell, C.D. Potter, A.J. Schultz, D.M. Young, J.D. Jorgensen, and S.D. Bader, J. Solid State Chem. **124**, 381 (1996).
[47] F. Damay, C. Martin, M. Hervieu, A. Maignan, B. Raveau, G. André, and F. Bourée, J. Magn. Magn. Mater. **184**, 71 (1998).
[48] This is particularly the case of the P phase. Knizek *et al.* (Ref. 18) and Kawano *et al.* (Ref. 19) reported the *Pbnm* orthorhombic structure. In contrast, Argyriou *et al.* (Ref. 46) and Damay *et al.* (Ref. 47) reported the $F4/mmmc$ and the $I4/mcm$ tetragonal symmetry, respectively. There is also some discrepancy in the Jahn-Teller distortion and Mn-O-Mn bond angles.
[49] This may be due to smaller orbital polarization above T_N in $Nd_{1/2}Sr_{1/2}MnO_3$ than that in $Pr_{1/2}Sr_{1/2}MnO_3$, and is consistent with the smaller Jahn-Teller distortion as observed above T_N in $Nd_{1/2}Sr_{1/2}MnO_3$ (Ref. 21).
[50] N. Fukumoto, S. Mori, N. Yamamoto, Y. Moritomo, T. Katsufuji, C.H. Chen, and S-W. Cheong, Phys. Rev. B **60**, 12 963 (1999).
[51] T. Asaka, Y. Anan, T. Nagai, S. Tsutsumi, H. Kuwahara, K. Kimoto, Y. Tokura, and Y. Matsui, Phys. Rev. Lett. **89**, 207203 (2002).